

Invited Review

Electrolyte and current collector designs for stable lithium metal anodes

Simeng Zhang^{1,2)}, Gaojing Yang^{1,3)}, Xiaoyun Li^{1,2)}, Yejing Li^{1,3)}, Zhaoxiang Wang^{1,2,3)},, and Liquan Chen¹⁾

1) Key Laboratory for Renewable Energy, Chinese Academy of Sciences, Beijing Key Laboratory for New Energy Materials and Devices, Institute of Physics, Chinese Academy of Sciences, Beijing 100190, China

2) College of Materials Science and Opto-Electronic Technology, University of Chinese Academy of Sciences, Beijing 100190, China

3) School of Physical Sciences, University of Chinese Academy of Sciences, Beijing 100190, China

(Received: 12 January 2022; revised: 16 February 2022; accepted: 21 February 2022)

Abstract: With the increasing demand for high energy-density batteries for portable electronics and large-scale energy storage systems, the lithium metal anode (LMA) has received tremendous attention because of its high theoretical capacity and low redox potential. However, the commercial application of LMAs is impeded by the uncontrolled growth of lithium dendrites. Such dendrite growth may result in internal short circuits, detrimental side reactions, and the formation of dead lithium. Therefore, the growth of lithium metal must be controlled. This article summarizes our recent efforts in inhibiting such dendrite growth, decreasing the detrimental side reactions, and elongating the LMA lifespan by optimizing the electrolyte structure and by designing appropriate current collectors. After identifying that the unstable solid electrolyte interface (SEI) film is responsible for the potential dropping in carbonate electrolytes, we developed $\text{LiPF}_6\text{-LiNO}_3$ dual-salt electrolyte and lithium bis(fluorosulfonyl)imide (LiFSI)–carbonate electrolyte to stabilize the SEI film of LMAs. In addition, we achieved controlled lithium deposition by designing the structure and material of the current collectors, including selective lithium deposition in porous current collectors, lithiophilic metal guided lithium deposition, and iron carbide induced underpotential lithium deposition in nano-cavities. The limitations of the current strategies and prospects for future research are also presented.

Keywords: lithium metal anode; electrolyte; current collector; lithium dendrite; solid electrolyte interface


1. Introduction

Since lithium-ion batteries (LIBs) were commercialized in 1991, they have achieved widespread adoption in consumer electronics, electric vehicles, and energy storage applications. However, LIBs using graphite-based anodes and lithium-containing cathodes are approaching their theoretical energy densities [1–2]. Therefore, secondary lithium batteries will play an important role in next-generation high energy-density batteries because of the high specific capacity ($3860 \text{ mAh}\cdot\text{g}^{-1}$) and the low redox potential (-3.04 V vs. SHE) of the lithium metal anode (LMA) [3–4]. In addition, the selection of the cathode materials will be significantly extended because lithium is not a required component of the cathode materials in secondary lithium batteries. However, the growth of lithium dendrites restricts the application of lithium metal batteries. The volume expansion during lithium deposition leads to breakage of the solid electrolyte interface (SEI) films, thereby allowing lithium dendrites to grow in the cracks of the SEI films or penetrate the SEI films directly. These lithium dendrites can impale the separator, leading to short circuiting of the batteries and even triggering thermal runaway. Moreover, lithium dendrites may aggravate the detrimental side reactions and cause the formation of “dead” lithium, thereby leading to low Coulombic efficiency and a

short lifespan [5–6]. Therefore, it is important to suppress the growth of dendrites and increase the stability and safety of lithium metal batteries.

Various models have been proposed to explain the growth behaviors of lithium metal, such as the phase-field model [7–10], the electrostatic shield model [11–14], and the SEI-induced nucleation model [15–18]. These models illustrate the many factors affecting the growth of the lithium dendrites, such as ion transport, current density, temperature, pressure, surface property, and electric field. The morphology of the deposited lithium can be improved by homogenizing the electric field distribution, promoting ion diffusion, and increasing mechanical pressure.

The currently reported strategies that effectively suppress dendrite growth can be classified into three categories: optimizing electrolyte structures [19–22], designing current collectors [23–26], and building artificial SEI films [27–30]. Various new liquid electrolytes have been designed to tune the properties of SEI films and to improve the LMA performance, such as fluorinated electrolytes [31–33], concentrated electrolytes [21,34], and electrolytes enhanced by additives [35–37]. Designing the current collectors with three-dimensional (3D) structures [38–40] and a lithiophilic surface [41–43] is an effective approach to regulating the lithium deposition and controlling both the position and morpho-

 Corresponding author: Zhaoxiang Wang E-mail: zxwang@iphy.ac.cn

© University of Science and Technology Beijing 2022

logy of the deposited lithium by modulating the electric field distribution and reducing the lithium nucleation barriers. There is a wide range of materials (e.g., alloys, polymers, gels, organics, inorganics, and organic–inorganic composites) and various approaches (coating/casting, vapor deposition, solution dipping, electrochemical treatment, chemical treatment, etc.) for constructing homogenous, ion-conductive, and stable artificial SEI films to suppress the uncontrolled lithium dendrite growth and accommodate the volume change of lithium metal [44–47].

In this article, we summarize our recent investigations on high-performance LMAs based on electrolyte optimization and current collector design. We first clarify the importance of a stable SEI film by exploring the reason for the potential dropping and develop LiPF_6 – LiNO_3 dual-salt electrolyte and lithium bis(fluorosulfonyl)imide (LiFSI)–carbonate electrolyte to form stable SEI films. Our works on designing current collectors to control the deposition of lithium metal are then presented: lithium deposition induced by (1) 3D current collectors, (2) lithiophilic alloys, and (3) iron carbides in carbon nanotube (CNT) cavities. Finally, conclusions and prospects are provided for further research on highly stable LMAs.

2. Electrolyte optimization to stabilize the SEI film

The electrolyte is a crucial factor that affects the Coulombic efficiency, lifespan, and deposition morphology of an LMA. The electrolyte is crucial in secondary lithium batteries because it is involved in the formation of an effective and stable SEI film on an LMA. An ideal SEI film has the following features: (1) high stability in structure and components, (2) high ion conductivity to ensure rapid ion transport, (3) mechanically robust and flexible to adapt to the large volume change of the LMA, and (4) appropriate thickness to prevent electron tunneling and decrease the electrode polarization. The composition of the electrolytes, the interaction between the various components, and their reduction potentials determine the properties of the SEI film on the LMA surface. Therefore, it is important to determine the relationship between the electrolyte structure and the SEI properties and to adjust the electrolyte components accordingly to achieve stable lithium plating/stripping.

2.1. Potential dropping and SEI evolution in the LiPF_6 EC/DMC electrolyte

Having wide electrochemical windows, carbonate-based electrolytes are attractive for the development of lithium metal batteries. However, the lithium deposition potential drops after some lithium deposition in carbonate-based electrolytes (Fig. 1(a)) [48], leading to low energy density, poor energy conversion efficiency, and overcharge of the battery. By physical characterization and electrochemical evaluation, we discovered that the potential dropping during lithium plating is caused by the decomposition of the commercial LiPF_6 ethylene carbonate (EC)/dimethyl carbonate (DMC) electro-

lyte and the formation of an unstable SEI film in it. The slight increase in the organic species ROCO_2Li in the SEI film during lithium plating (Fig. 1(b)) produces a significant increase in charge transfer resistance (Fig. 1(c)) and a sharp drop in the lithium plating potential, causing severe battery polarization. In addition, the organic species (ROCO_2Li and ROLi) in the SEI film are decomposed into several inorganic species, such as Li_2CO_3 and Li_2O , during lithium dissolution, damaging the SEI integrity. Therefore, electrolyte decomposition and SEI film re-formation lead to the dropping of the lithium plating potential during the charge/discharge cycles. The potential does not drop anymore after several cycles because the accumulated Li_2CO_3 and Li_2O become sufficiently compact during cycling and can effectively separate the deposited lithium from the carbonate electrolyte. However, the polarization of the battery increases as the SEI thickness rises in this process.

These findings explain the origin of the potential dropping and reveal the important impact of the SEI film on the lithium plating/stripping behavior. Therefore, obtaining a thin and stable SEI film by optimizing the electrolyte composition is critical in improving the performance of secondary lithium metal batteries.

2.2. LiPF_6 – LiNO_3 dual-salt electrolyte

LiNO_3 is a popular additive used in ether electrolytes [49–50], in which the NO_3^- anions are engaged in the lithium ion solvation and form a Li_3N -rich SEI film as they are reduced on the anode surface. However, the low solubility of LiNO_3 in carbonate solvents limits its application. We obtained a stable SEI film and improved the cycle performance of a lithium metal battery by constructing a LiPF_6 – LiNO_3 dual-salt electrolyte via mixing the LiNO_3 –tetraethylene glycol dimethyl ether (TEGDME) solution and the LiPF_6 –EC/DMC electrolyte [51]. A mechanism of anion competition was proposed to understand the interactions between the different components in the dual-salt electrolyte. As the PF_6^- anions are replaced with the NO_3^- anions in the Li^+ solvation shell, more NO_3^- anions are reduced to form a Li_3N -rich SEI film; however, PF_6^- decomposition is inhibited in the dual-salt electrolyte (Fig. 2(a)–(e)). The suppressed leaching effect of the acidic components (PF_5 and HF) from LiPF_6 to the SEI film (Fig. 2(f) and (g)) is beneficial for the formation of a compact and stable SEI film and the decrease of the side reactions between the lithium metal and the electrolyte. Furthermore, the LiNO_3 -conducted ionically conductive Li_3N in the SEI film modulates the lithium nucleation morphology (Fig. 2(h)) and promotes the deposition of dense and dendrite-free lithium metal. These improvements were demonstrated in a $\text{Li}||\text{Cu}$ cell that ran stably for 210 cycles with Coulombic efficiencies over 97% (Fig. 2(i)).

2.3. LiFSI–carbonate electrolyte

Although the commercial LiPF_6 –carbonate electrolyte matches well the high-voltage cathode materials, the SEI film derived from it is unstable against the attack of lithium metal. As an important component of the SEI film, LiF has a high

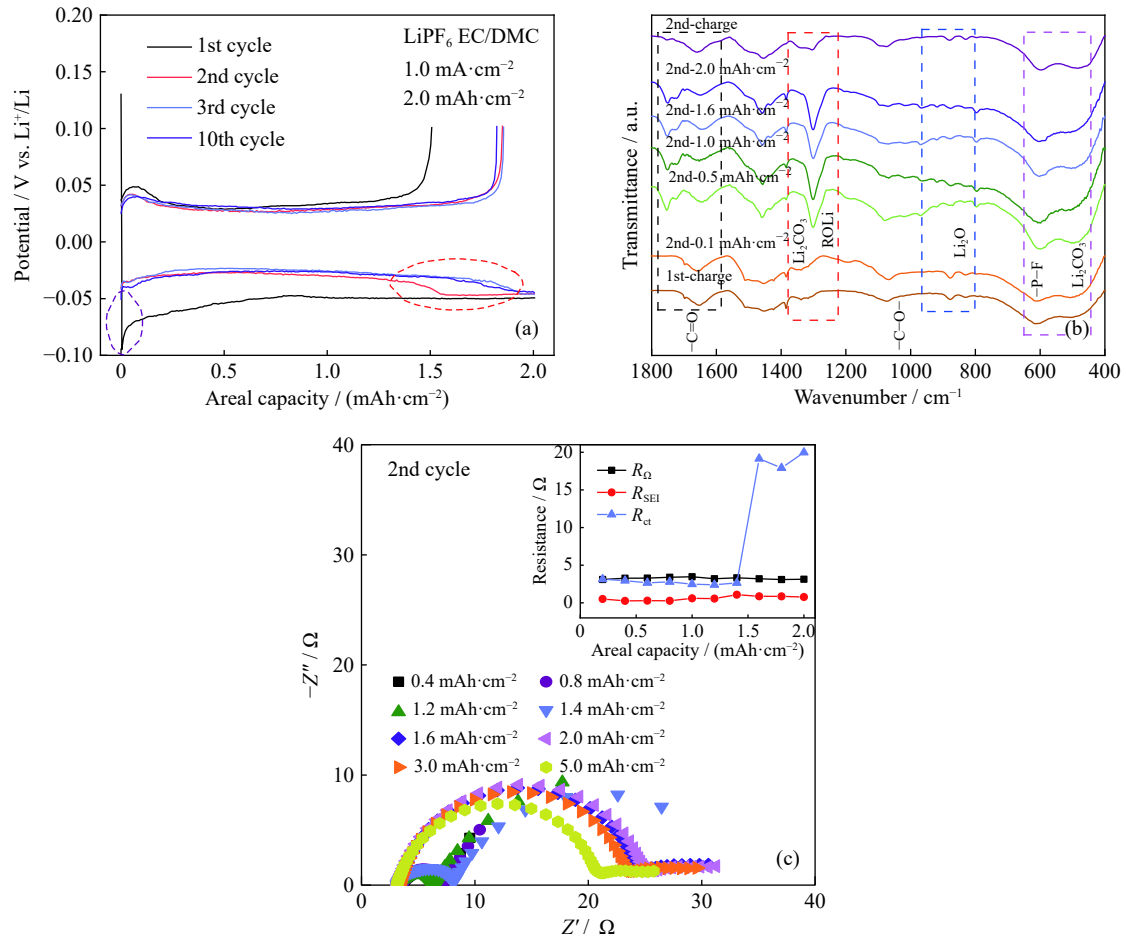


Fig. 1. (a) Lithium plating/stripping potential profiles in the LiPF₆ EC/DMC electrolyte, (b) Fourier-transformed infrared (FTIR) spectra of the SEI film and (c) the impedance spectra at different lithium plating/stripping capacities in the second cycle (the insets: the fitting results of the impedance spectra; R_{Ω} , R_{SEI} , and R_{ct} are the ohmic resistance, the SEI layer resistance, and the charge transfer resistance, respectively). Reprinted from *Nano Energy*, 70, S.M. Zhang, G.J. Yang, S. Liu, *et al.*, Understanding the dropping of lithium plating potential in carbonate electrolyte, 104486, Copyright 2020, with permission from Elsevier.

shear modulus (55.1 GPa) and is chemically stable against lithium metal and organic electrolytes [52]. The presence of LiF is conducive to LMA stabilization, thereby allowing for high Coulombic efficiency and cycle stability [31–32]. Replacing LiPF₆ with LiFSI in the carbonate electrolyte, we obtain a stable and compact LiF-rich SEI film [53]. This film effectively prevents the side reactions between the deposited lithium and the carbonate solvent. The deposited lithium particles remain dense after 50 cycles (Fig. 3(a)–(c)). The Li|Cu cell maintained a Coulombic efficiency of 95.5% after 95 cycles (Fig. 3(g)), and the Li|Li₄Ti₅O₁₂ full cell with a limited amount of lithium loading also exhibited an excellent cycling performance in the LiFSI electrolyte. In contrast, voids are observed in the SEI film in the LiPF₆ electrolyte due to the leaching effect of the LiPF₆ decomposition products. As a result, the deposited lithium was found to be porous, and more dead lithium was observed (Fig. 3(d)–(f)).

Graphite is a typical anode material used in LIBs because of its high structural stability caused by the presence of a stable SEI film in the carbonate-based electrolyte. Graphite is also a promising material of current collectors for an LMA battery because it is lithiophilic after lithium intercalation [54]. However, graphite becomes very vulnerable against the

co-intercalation of the solvated Li⁺ ions if the SEI film on it is damaged, for example, by the lithium metal. The LiFSI–carbonate electrolyte was found to be superior on a natural graphite (NG) substrate [55]. The Coulombic efficiency of the Li|NG cell was found to rise sharply to 93.5% in a few cycles and remain stable thereafter for more than 70 cycles in the LiFSI electrolyte, whereas it was found to decrease sharply after 30 cycles in the LiPF₆–carbonate electrolyte (Fig. 3(h)). The superiority of the LiFSI electrolyte was found to be even more significant at elevated temperatures (60°C). The performance difference is attributed to the leaching effect of the LiPF₆ decomposition products and the increased LiF content in the SEI film formed in the LiFSI-based electrolyte. In the LiFSI electrolyte, the FSI⁻-derived SEI film that remains stable and compact under the lithium deposition potential can effectively protect the graphite and the deposited lithium and reduce side reactions, thereby improving the Coulombic efficiency and cycle stability (Fig. 3(k) and (l)).

Molecular dynamics calculations demonstrated that, in comparison with the LiPF₆ electrolyte, there are more anions in the Li⁺ solvation shell in the LiFSI electrolyte (Fig. 3(i) and (j)). FSI⁻ can be decomposed to form LiF and other FSI⁻-de-

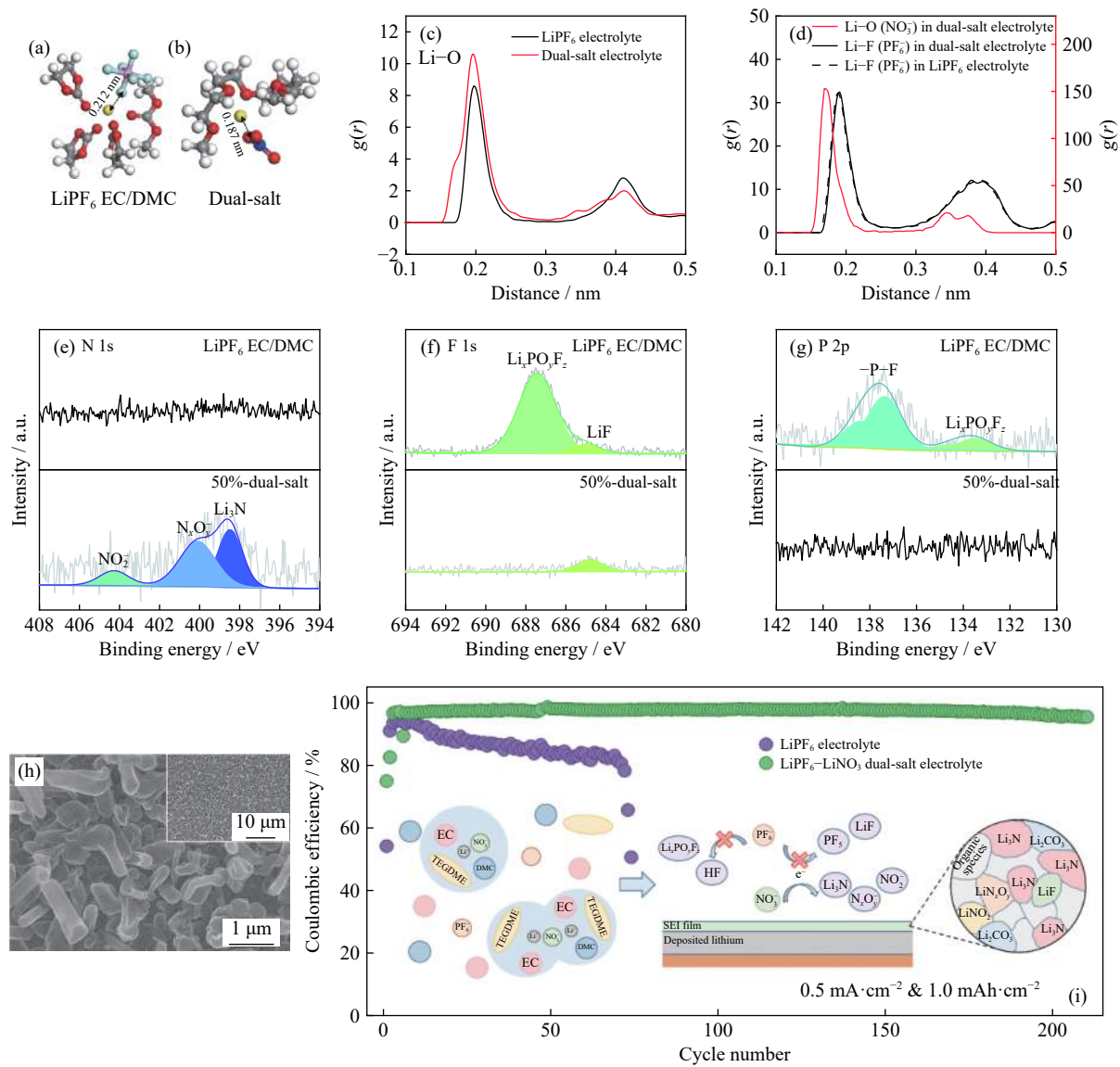


Fig. 2. Schematics of the Li-ion solvation structures in the LiPF_6 electrolyte (a) and in the $\text{LiPF}_6\text{-LiNO}_3$ dual-salt electrolyte (b). Note the color code for the different elements: white for hydrogen, yellow for lithium, gray for carbon, red for oxygen, blue for nitrogen, green for fluorine, and purple for phosphorus. (d) Radial distribution functions ($g(r)$) of Li-O (c), Li-O (NO_3) and Li-F (PF_6). X-ray photoelectron spectroscopy (XPS) results of the SEI components in the LiPF_6 electrolyte and in the dual-salt electrolyte after 30 cycles: N 1s (e), F 1s (f), and P 2p (g) spectra. (h) Morphology of the deposited lithium in the dual-salt electrolyte. (i) Electrochemical performances in the LiPF_6 and dual-salt electrolytes along with the schematic illustration of the effect of the Li-ion solvation structures on the deposition of lithium metal. Reprinted with permission from S.M. Zhang, G.J. Yang, Z.P. Liu, *et al.*, *Nano Lett.*, 21, 3310-3317 (2021) [51]. Copyright 2021 American Chemical Society.

rived species during lithium plating, forming a compact and stable SEI film. Minimizing the particle size of the graphite can further lessen the particle pulverization, thus boosting the Coulombic efficiency and cycle lifespan [55–56].

The inactive lithium in the form of the SEI film and electrically isolated metallic lithium (more frequently called dead lithium) has been identified as the main origin of the capacity decay and the restricted lifespan [57]. We used LiFSI-carbonate electrolyte and $\text{LiPF}_6\text{-LiNO}_3$ dual-salt electrolyte to suppress the formation of the SEI film and dead lithium, significantly improving the Coulombic efficiency and lifespan of the cell. Fang *et al.* [58] reported the use of the titration gas chromatography technique to quantify the contribution of the dead lithium and SEI formation to the total irreversible Cou-

lombic efficiency and proposed ideal architectures of the deposited lithium and SEI film. The deposited lithium should retain a columnar microstructure with a large granular size and minimum tortuosity to minimize the unreacted metallic lithium residue. The SEI film should be chemically and spatially homogeneous to ensure uniform Li^+ dissolution and mechanically elastic enough to accommodate the volume change. We recently demonstrated that these requirements can be met by using advanced electrolytes, such as the LiFSI-carbonate electrolyte and the $\text{LiPF}_6\text{-LiNO}_3$ dual-salt electrolyte. In addition to the advanced electrolytes, the 3D frameworks that maintain electronic pathways can contribute to establishing a durable structural connection to decrease the amount of electrically isolated metallic lithium. Lithiophilic

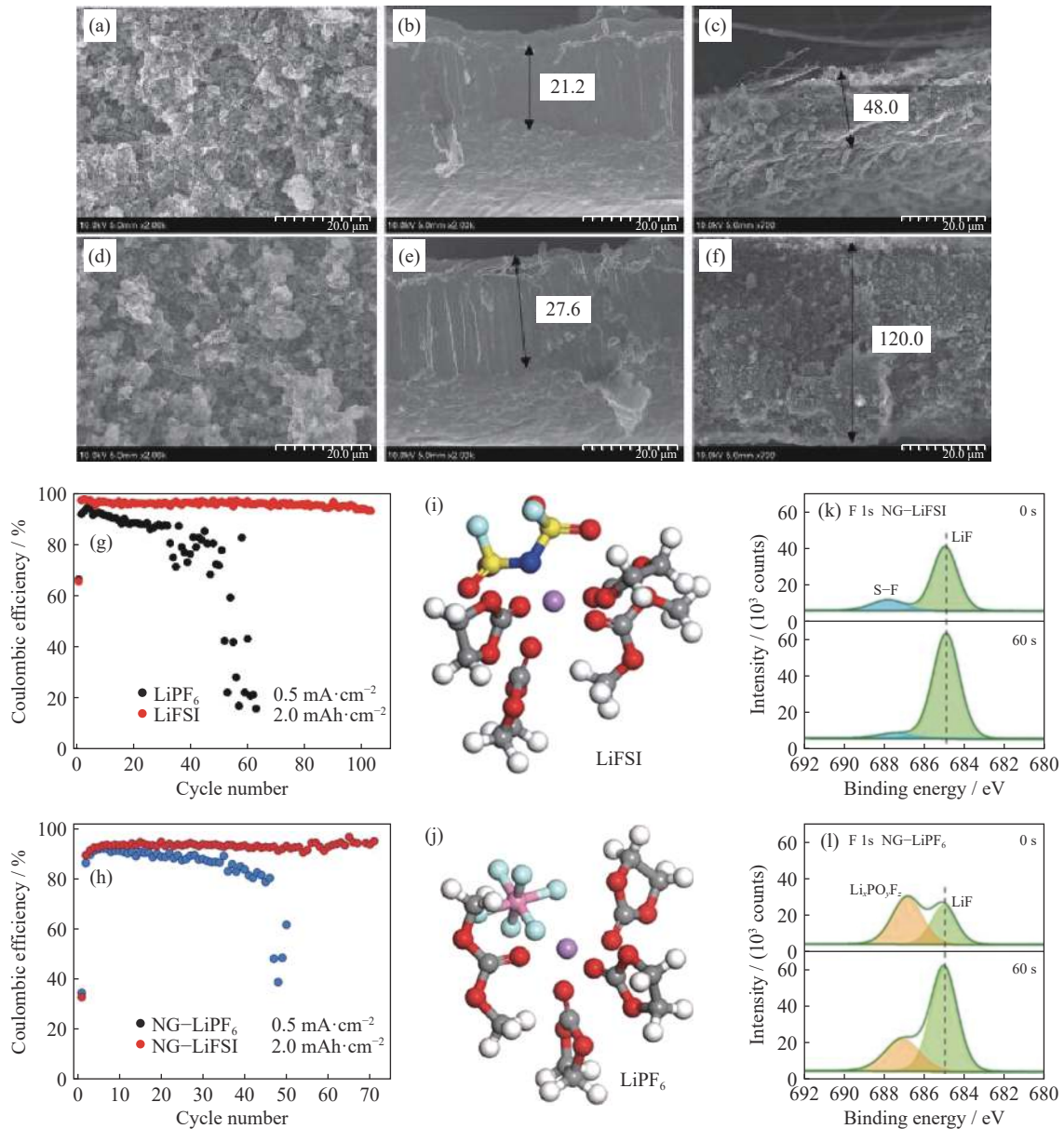


Fig. 3. Surface (a, d) and cross-section (b, c, e, f) views of the deposited lithium on the planar Cu current collector (b, e) and the dead lithium on the porous glass fiber (c, f) after 50 cycles in the LiFSI electrolyte (a–c) and in the LiPF₆ electrolyte (d–f). Comparison of the Coulombic efficiencies of the Li|Cu cells (g) and the Li|NG cells (h) using the LiFSI and LiPF₆ electrolytes. For convenience, the Li|NG cells using the LiFSI and LiPF₆ electrolytes are noted as the NG–LiFSI cell and the NG–LiPF₆ cell, respectively. (i, j) Calculated Li-ion solvation structures (red for oxygen, gray for carbon, white for hydrogen, purple for lithium, dark blue for nitrogen, yellow for sulfur, light blue for fluorine, and pink for phosphorus). XPS results of the SEI components on the graphite in the LiFSI (k) and LiPF₆ (l) electrolytes during the 20th lithium plating cycle. (a–g) Reprinted from *Energy Storage Mater.*, 23, G.J. Yang, Y.J. Li, S. Liu, S.M. Zhang, Z.X. Wang, and L.Q. Chen, LiFSI to improve lithium deposition in carbonate electrolyte, 350–357, Copyright 2019, with permission from Elsevier. (h–l) Reprinted with permission from G.J. Yang, S.M. Zhang, S.T. Weng, et al., *Nano Lett.*, 21, 5316–5323 (2021) [55]. Copyright 2021 American Chemical Society.

substrates are conducive to the formation of lithium deposits with a large granular size via energetically favorable lithium nucleation on the lithiophilic metals or alloys.

3. Current collector design to control lithium deposition

The texture of the current collector strongly affects the behavior of lithium deposition and dissolution. Two strategies have been developed to modulate the lithium plating/strip-

ping behavior by specially designing 3D current collectors to adjust the electric field distribution and introduce lithiophilic materials to reduce the nucleation barrier.

3.1. Lithium deposition in porous current collectors

Many studies have shown that the lithium plating/stripping behaviors are related to the physical and (electro)chemical properties of the electrode surface. However, a fundamental understanding of how the electrode surface morphology affects the lithium deposition behavior remains lacking.

We found that the electrochemical activity of the porous electrode becomes less important than the specially designed porous structure of the electrode in the position of lithium deposition. For example, the lithium deposition can be guided in the micro-grooves on a Ti foil (Fig. 4(a) and (b)) [59]. With this phenomenon as a start, we further found that lithium metal is preferentially deposited in the micropores with different physical and chemical properties; for example, the micro-fabricated wells on a Si wafer and hydrothermally grown ZnO nanowire arrays through both Si (Li-Si alloying) and ZnO (Li⁺-ZnO conversion reaction and Li-Zn alloying) are electrochemically active for lithium storage. The lithium initially nucleates on the bottom of the well and then grows in it (Fig. 4(c) and (d)). In addition to the physical pits, the gaps or cracks between the ZnO nanowire arrays function as natural nanopores and allow the deposited lithium to accumulate in them before the conversion reaction occurs (Fig. 4(e) and (f)). We proposed a mechanism to explain the preferential lithium deposition in these pits. A pit on the current collector is reverse to a protrusion of the electrolyte. Obviously, according to classical electromagnetism principles, the tip of the electrolyte is the point where Li⁺ ions gather and the cur-

rent is the strongest. As a result, most of the Li⁺ ions can accept electrons and preferentially be deposited in the pits. Thus, controlled lithium deposition can be achieved by specially designing the geometric structure of the current collectors.

Extending the above results to porous current collectors, higher-capacity lithium metal deposition can be realized with high Coulombic efficiencies. With the commercial carbon nanotube sponge (CNTs) as a porous current collector, the electrochemical performance of LMAs was improved [60]. With the high specific surface area of CNTs, the lithium nucleation site increases and the local current density decreases, thus ensuring uniform lithium deposition. The investigation of the morphology evolution during lithium plating shows that lithium is initially uniformly deposited on the CNT framework and then fills the voids in the sponge network gradually (Fig. 4(g)). The CNT sponge can accommodate up to 10.0 mAh·cm⁻² of lithium without lithium dendrites. In addition, the lithium nucleation overpotential decreases because of the lithium affinity of the lithium-intercalated CNTs (Fig. 4(i)). Moreover, the lithium plating/stripping on the

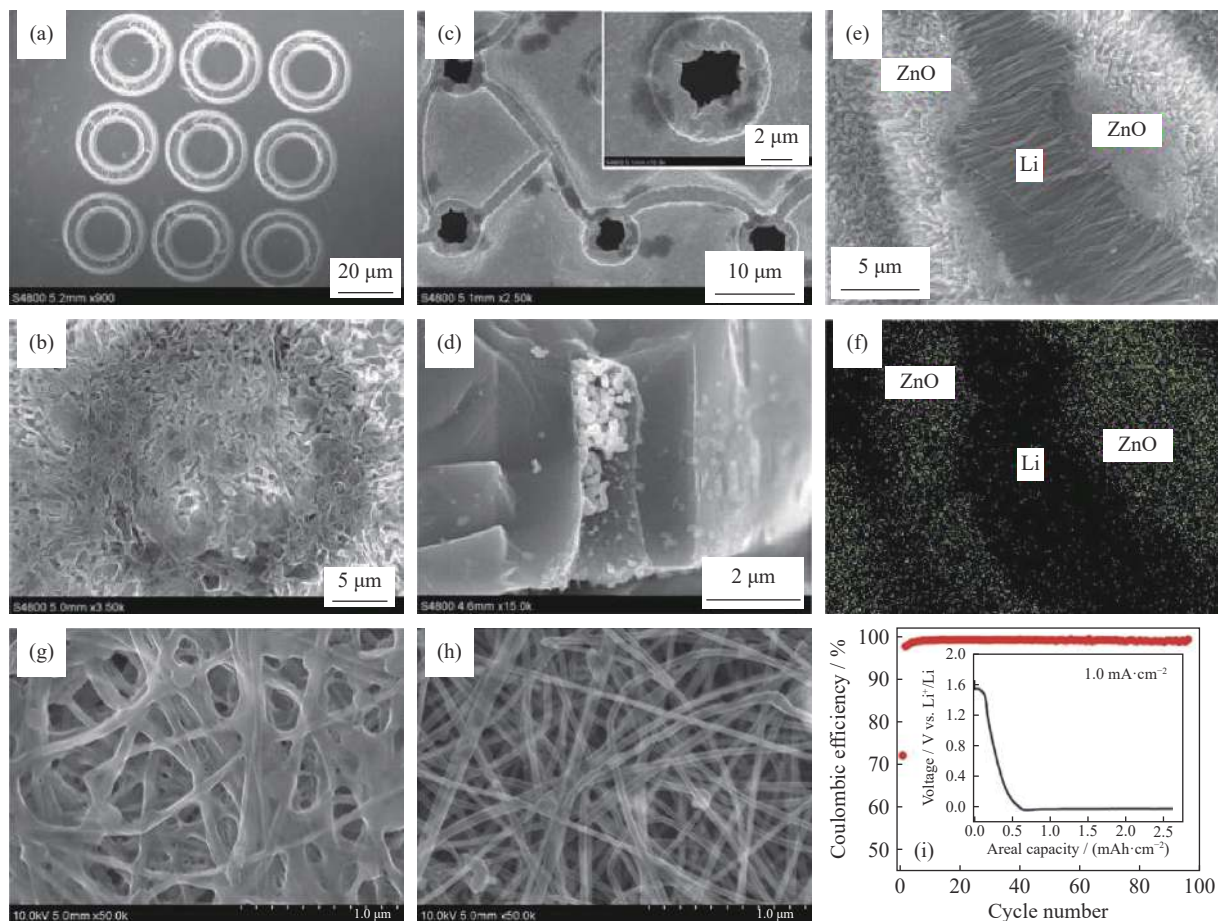


Fig. 4. SEM images of the micro-patterned Ti foil (a, b) and Si pattern (c, d) prepared by micro/nano-fabrication technology before (a) and after (b–d) lithium plating. SEM image of the Li nanowires array grown between the ZnO arrays (e) and the corresponding EDS mapping (f). (a–f) Reprinted from *Nano Energy*, 23, Y.J. Li, J.Y. Jiao, J.P. Bi, X.F. Wang, Z.X. Wang, and L.Q. Chen, Controlled deposition of Li metal, 241–246, Copyright 2017, with permission from Elsevier. Morphologies of the CNT sponge at the lithium plating capacity of 2.0 mAh·cm⁻² in the first cycle (g) and lithium stripping after 20 cycles (h). (i) Coulombic efficiencies and the lithium plating/stripping potential profiles of the Li||CNTs cell. (g–i) Reprinted with permission from G.J. Yang, Y.J. Li, Y.X. Tong, et al., *Nano Lett.*, 19, 494–499 (2019) [60]. Copyright 2019 American Chemical Society.

CNT sponge maintains high efficiency and cycle stability in the ether electrolyte on account of the graphite-amorphous carbon composite structure (Fig. 4(h)). The Li||CNTs cell was found to run stably for 400 h with efficiencies over 98.5% (Fig. 4(i)). The co-intercalation of the solvated Li^+ and the exfoliation of the layer-structured graphite are inevitable in the ether-based electrolytes. Therefore, this composite structure is vital to the structural stability of CNTs.

3.2. Lithiophilic metal guided lithium deposition

The pre-lithiation behavior of the carbon materials enhances their affinity for lithium metal. However, the lithium nucleation barriers are still large [60–61], thus hindering the uniform lithium deposition. By coating nano-sized Ag particles on commercial carbon fiber paper (CP; CP@Ag) (Fig. 5(a) and (b)) [62], we improved the lithium plating/stripping performance. The lithiophilic and uniformly distributed Ag particles are able to alloy with lithium and guide uniform lithium deposition on the carbon fiber, thereby effectively alleviating the polarization and boosting the energy conversion efficiency of the LMA. The nucleation and deposition overpotentials were found to decrease from 35 and 26 mV on CP to 21 and 18 mV on CP@Ag in the first cycle, respectively (Fig. 5(c) and (d)). The Li||CP@Ag half-cell was found to stably cycle for about 1000 h at a current density of $0.5 \text{ mA} \cdot \text{cm}^{-2}$. The improved cycling stability is attributed to the strong adhesion of the plated silver particles on the carbon fiber.

In addition to Ag, other lithiophilic metals can decrease the nucleation overpotential and contribute to uniform lithium deposition, such as Zn [63–64], Al [65–66], and Mg [67–68]. These findings indicate that the lithium plating/stripping behaviors are closely related to the substrate materials, including the nucleation overpotential, the morphology of the deposited lithium (or alloys), and the cycle performance. The reasons for these differences, however, remain unclear. Therefore, the principle for the rational selection of the substrate materials remains lacking. We characterized a series of lithiophilic materials and found an interesting relationship between the lithium deposition/dissolution behavior and the phase transition process (the lithium metal binary phase diagram) (Fig. 5(g)–(j)) [69]. The metals whose phase diagrams exclude intermetallic compounds can constantly accept lithium to form solid solutions, e.g., Ag and Mg. During the lithium deposition/dissolution on the Ag@Cu substrate, phase transitions of Li–Ag alloys are always observed. The lithium ions are reduced to Li–Ag solid solutions instead of free lithium metal during lithium deposition. In contrast, the (non)metals of whom the phase diagrams include intermetallic compounds (such as Au, Al, Zn, Si, and Sn) do not undergo phase transitions any longer after the formation of the lithium-saturated intermetallic compounds; the deposited lithium exists in the form of free lithium metal. Therefore, the Au element only appears on the surface of the Cu foil, and the free lithium lies between the lithium-saturated alloy and the SEI film.

Density functional theory (DFT) calculations illustrated that the diffusion barrier of lithium in the Li_3Ag alloy and that in the Li_3Au alloy are similar. This finding rules out the possibility that the above difference in the alloying/de-alloying behavior is associated with the kinetic factors (such as the current density or deposition rate) and proves that the difference is determined by thermodynamic factors (the phase diagram).

Based on the relationship between the phase diagram and the lithium deposition behavior, we classified the lithiophilic materials into two categories. The metals that only form solid solutions with lithium can accommodate a large amount of the deposited lithium with small structural changes, ensuring the stability and integrity of the host (the metal substrate) during repeated alloying/de-alloying. These metals can guide the lithium plating/stripping throughout the cycling process (Fig. 5(e) and (f)). In contrast, the (non)metals that contain intermetallic compounds in their phase diagrams can no longer adjust the morphology of the deposited lithium after they are covered with free lithium metal. The internal strain accumulated during the two-phase transition promotes the fragmentation of the metal substrate, resulting in poor lithium plating/stripping cycling stability (Fig. 5(f)). These findings can be applied to predict the electrochemical performance of (non)metal substrates in lithium metal batteries and other secondary metal batteries, as well as direct the rational design of these substrates.

3.3. Iron carbide induced underpotential lithium deposition in nano-cavities

Lithium (and sodium) deposition in the micropores is an interesting approach for the development of an active lithium (and sodium) storage material or a porous current collector. Although some researchers claimed that they realized lithium (and sodium) storage in porous carbons [70–73], no solid evidence was provided, leaving it an open question whether lithium (and sodium) can be stored in the micropores. By inducing lithium with lithiophilic materials, we realized lithium storage in the CNT nano-cavities (Fig. 6(a) and (b)) and directly observed it using the cryogenic transmission electron microscopy (cryo-TEM) technique [74]. DFT calculations indicated that the iron carbides (Fe_xC) in the cavity have a strong affinity for lithium and sodium. The characteristic lattice fringes for lithium (Fig. 6(c), (e), and (f)) by cryo-TEM and the characteristic energy loss peak around 55 eV observed by cryo-electron energy loss spectroscopy (EELS) (Fig. 6(d)) confirmed the presence of lithium metal in the CNT cavities. By experimental characterization and theoretical calculations, this study demonstrated the potential for lithium storage within CNT cavities. However, no sodium was detected in the Fe_xC -containing CNT cavities. Based on these studies, we proposed three prerequisites for metal storage: (1) lithium ions can diffuse in the host material, (2) lithium ions can pass through the graphene layer through defects, and (3) the inducing species exist in the nano-cavity. No lithium metal was observed around the CNT openings or iron

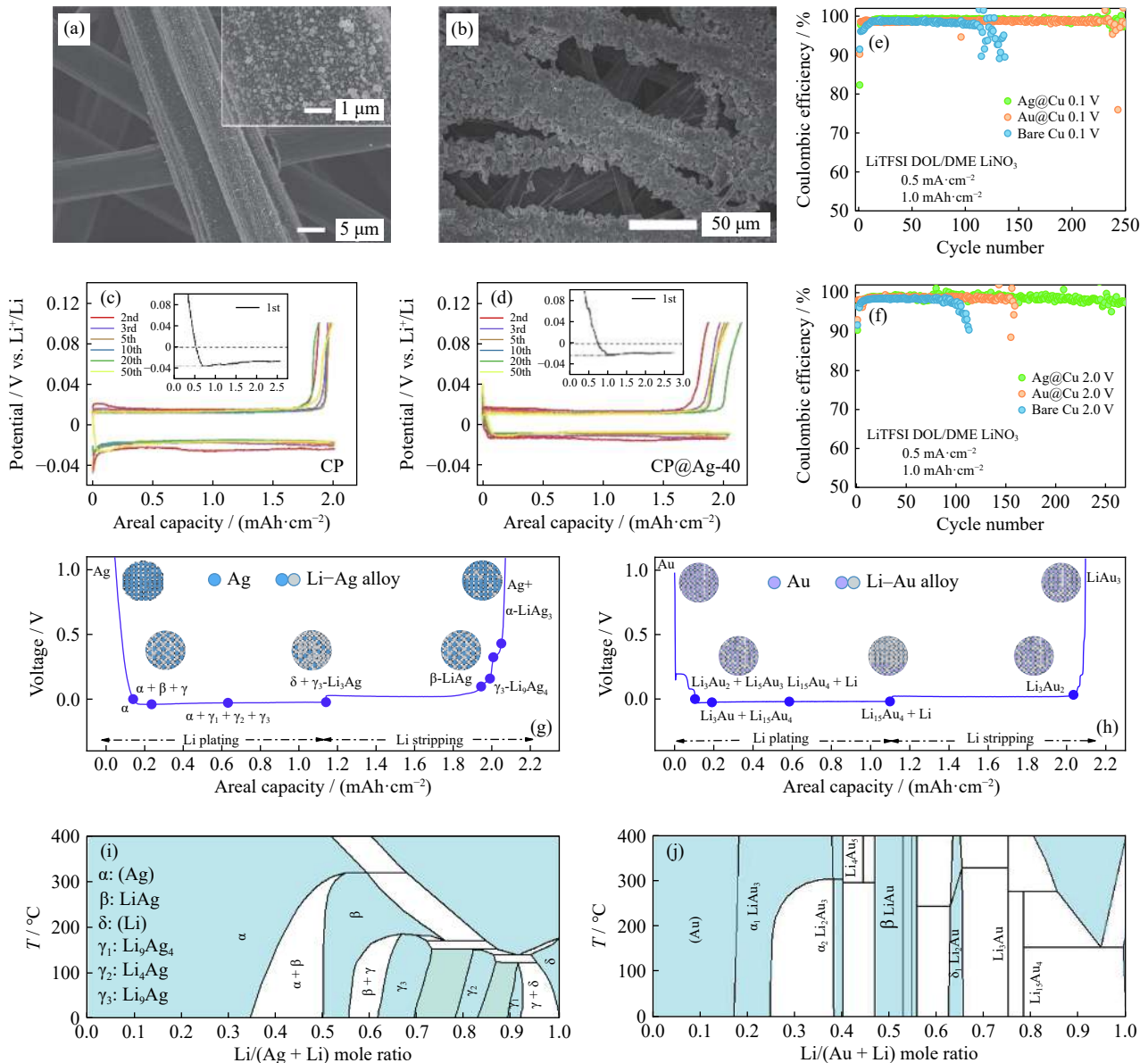


Fig. 5. Morphologies of the CP@Ag before (a) and after lithium plating for $2.0 \text{ mAh}\cdot\text{cm}^{-2}$ (b). Electrochemical performances of the cells with CP (c) and CP@Ag (d) as the lithium deposition occurs on the substrates. (a–d) Reprinted from *Nano Energy*, 66, X.Y. Li, G.J. Yang, S.M. Zhang, Z.X. Wang, and L.Q. Chen, Improved lithium deposition on silver plated carbon fiber paper, 104144, Copyright 2019, with permission from Elsevier. Coulombic efficiency of the Li||Cu cells with Ag@Cu, Au@Cu, and Cu substrates and the charge cutoff potentials of 0.1 V (e) and 2.0 V (f), with $1 \text{ mol}\cdot\text{L}^{-1}$ lithium bis(trifluoromethane)sulfonamide (LiTFSI) dissolved in 1,3-dioxolane (DOL) and 1,2-dimethoxyethane (DME) (1:1 in volume ratio) with 1wt% LiNO_3 additive as the the electrolyte. Schematic illustration of the phase transition on the Ag@Cu (g) and Au@Cu (h) substrates. Li–Ag (i) and Li–Au (j) binary phase diagrams. (e–j) Reprinted with permission from S.M. Zhang, G.J. Yang, Z.P. Liu, *et al.*, *ACS Energy Lett.*, 6, 4118–4126 (2021) [69]. Copyright 2021 American Chemical Society.

carbide-free regions, i.e., the iron carbide promotes the lithium ions to diffuse in the CNT interlayer and eventually reach the inside of CNTs through the defective graphene layer. No sodium was found in the cavities because the sodium ions cannot intercalate into CNTs. The three prerequisites can be used to promote concepts for lithium metal storage within the micro-nanopores of carbon materials and other porous materials.

There are two aspects for optimizing current collector design, structure and texture. Porous current collectors can modify the electric field distribution in the electrolyte via its

conductive surface structure and modulate the Li^+ ion concentration gradient in the electrolyte by reducing the local current density. The texture of the current collector is another key factor that affects lithium deposition. The lithiophilic materials can reduce the nucleation barrier for the heterogeneous lithium nucleation, thereby decreasing the nucleation overpotential. Moreover, the interaction between the lithiophilic materials and Li^+ ions enables a homogeneous distribution of the Li^+ ions, leading to a uniform lithium deposition. In fact, for the ultimate design of current collectors, the two strategies are usually combined to ensure both the low

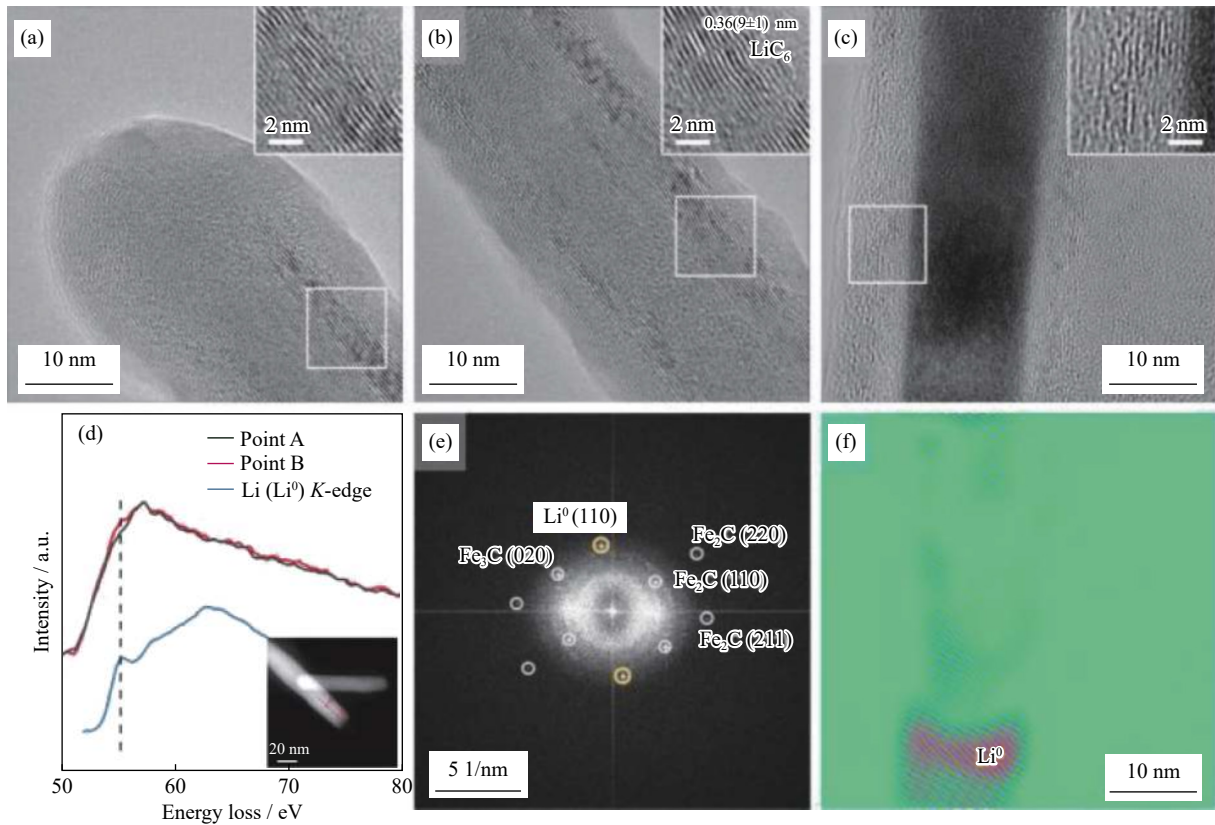


Fig. 6. Cryo-TEM images (a–c) and EELS line-scan spectra (d) of the CNTs discharged to 0.0 V (the insets are magnified views of the white square areas; point A and B refer to the white square areas of (a) and (b), respectively); fast Fourier-transformed (FFT) pattern (e) of (c) and inverse FFT image (f) of metallic lithium in (e). Reprinted from *Energy Storage Mater.*, 36, G.J. Yang, Z.P. Liu, S.T. Weng, *et al.*, Iron carbide allured lithium metal storage in carbon nanotube cavities, 459–465, Copyright 2021, with permission from Elsevier.

local current density and the high lithiophilicity of the current collector, such as using lithiophilic alloys as the 3D current collectors and plating lithiophilic metals on the 3D lithiophobic current collectors to reduce the lithium nucleation barriers, preloading lithium into the porous current collectors with lithiophilic interface layer to prepare composite electrodes, and arranging the positions of the lithiophilic/lithiophobic materials on the 3D frameworks to guide homogeneous and bottom-up lithium deposition.

4. Conclusions and outlooks

This article summarizes our recent efforts on the modification and protection of the LMA by rational electrolyte optimization and current collector design. We first discovered that the instability of the SEI film at the charged (lithium stripped) state is responsible for the potential dropping during the subsequent lithium deposition in the carbonate electrolytes. As a result, two electrolytes were developed to stabilize the SEI films in the carbonate electrolytes. First, a $\text{LiPF}_6\text{-LiNO}_3$ dual-salt electrolyte was designed to form a stable Li_3N -rich SEI by exploiting the competition between PF_6^- and NO_3^- anions in the Li-ion solvation structure. Second, LiFSI was used to replace LiPF_6 to ensure a compact and stable SEI film in the carbonate electrolyte, enhancing the stability of the deposited lithium on Cu foil and

graphite substrates. Realizing that lithium deposition can be controlled via the real or virtual pores of the micro-nano patterned substrate, we proposed minimized graphite, commercial CNT sponge, and CP as the porous substrate to improve the deposition and stripping of a large areal capacity of dendrite-free lithium. We then chemically coated the CP with silver nanoparticles to further reduce the lithium nucleation barrier on the porous substrate. Principles for the rational selection of lithiophilic metal substrates were proposed according to the presence or absence of intermetallic compounds in the lithium–(non)metal binary phase diagrams. We successfully stored metallic lithium in the nano-cavities of CNTs by virtue of the induction effect of lithiophilic Fe_3C . The results of these fundamental studies provide important guidance for the design and development of the electrolytes, SEI films, and current collectors of long-life secondary lithium batteries.

Regarding the directions of future research for lithium deposition and protection, we believe more attention should be paid to the following aspects.

(1) Design of the electrolyte components. The polarization, interfacial stability, and morphology of the deposited lithium are closely related to the electrolyte properties, such as the conductivity, the transference number and the diffusion coefficient of the Li^+ ions, and the decomposition potential of the electrolyte. It is time-consuming to identify appropriate electrolytes in a vast space of chemical systems using

the conventional trial-and-error approach. Hence, the mechanisms by which these properties affect the electrochemical performance must be clarified in order to build general electrochemical criteria for the construction, selection, and optimization of electrolytes. The microstructure of the electrolyte (the interactions between the components in the electrolyte, the Li^+ solvation structure, and the transport mechanism of the charge carriers) is another aspect to consider. Determining the solvation structure in electrolytes can assist in effective modification of the macro properties of an electrolyte by controlling the interaction of the components at the molecular level. For example, the addition of diluent solvents can change the concentration distribution of the effective lithium ions to design the locally concentrated electrolytes; this approach holds the advantages of both the broad electrochemical windows of the concentrated electrolytes and the low viscosity of the diluent electrolytes.

(2) Structural design and material selection of the current collectors. Although it is well accepted that 3D porous current collectors can suppress dendrite growth and elongate the lifetime of a lithium anode, a clear correlation between the texture of the current collector and the lithium deposition/dissolution has not been established. The geometric parameters of 3D current collectors, including the pore structure and pore volume, the specific surface area, and the lithium loading, must be reasonably considered for practical applications. Although the electrochemical behaviors of lithiophilic (non)metals can be predicted via phase diagrams, a further fundamental understanding of the effect of current collectors on the growth of lithium metal is required. Further investigation is required on the impact of the various factors on lithium deposition, such as the hardness, wettability, surface energy, and geometry of the current collectors. In addition, the texture of the current collector also significantly affects the SEI composition on Cu and Ag substrates [64], possibly via the catalysis of electrolyte decomposition by Ag nanoparticles to the electrolytes decomposition. Understanding the correlation between the SEI film and the current collector chemistry, geometry, and mechanics can contribute to finding appropriate current collectors for LMAs.

(3) Composition and structure of the SEI film. The uniformity of ion diffusion in the SEI film depends on the distribution of the organic and inorganic species in the SEI film. A Li_3N -rich SEI film is beneficial for the formation of spherical lithium deposits via the enhanced Li^+ conductivity of the SEI layer. In addition, the composition and structure of the SEI film affect the lithium deposition behavior via its interaction with the solvated lithium ions and therefore determine the de-solvation energy barrier. Moreover, the side reactions between lithium and the electrolyte are associated with the compactness of the SEI film. Therefore, the role of each component in the SEI film and the interaction between these components on the properties of the SEI film deserve attention. In fact, the SEI film is the most complicated component because it is associated with both the electrolyte and the current collector and thus affects the lithium deposition and the

interaction between the electrolyte and the deposited lithium or the current collector. The SEI film structure and composition are complex, fragile to slight exterior disturbance, and difficult to characterize. New technologies must be developed to characterize the SEI film.

(4) Advanced characterization techniques. To gain fundamental insights into the lithium dendrite and SEI film formation mechanism in various current collectors and new electrolytes, advanced characterization techniques are urgently needed to monitor lithium dendrite growth and interphase evolution [75–76]. Examples of advanced characterization techniques are cryo-TEM, time-of-flight secondary ion mass spectrometry, *in situ* SEM/TEM/atomic force microscopy, and theoretical calculations. For instance, Cryo-TEM can characterize the composition and structure of SEI films that are sensitive to electron beams and air. *In situ* techniques can be used to track the real lithium plating/stripping process in a working cell, thereby elucidating the mechanism of dendrite nucleation and growth.

Integration of these strategies (and probably more) is expected to promote the realization of controllable adjustment of the lithium deposition kinetics and thermodynamics and products that meet the requirements of lithium metal batteries.

Acknowledgement

This work was financially supported by the National Natural Science Foundation of China (No. 21773301).

Conflict of Interest

The authors have no competing interests to declare that are relevant to the content of this article.

References

- [1] B. Liu, J.G. Zhang, and W. Xu, Advancing lithium metal batteries, *Joule*, 2(2018), No. 5, p. 833.
- [2] Y.C. Fan, X. Chen, D. Legut, and Q.F. Zhang, Modeling and theoretical design of next-generation lithium metal batteries, *Energy Storage Mater.*, 16(2019), p. 169.
- [3] W. Xu, J.L. Wang, F. Ding, *et al.*, Lithium metal anodes for rechargeable batteries, *Energy Environ. Sci.*, 7(2014), No. 2, p. 513.
- [4] X.B. Cheng, R. Zhang, C.Z. Zhao, and Q. Zhang, Toward safe lithium metal anode in rechargeable batteries: A review, *Chem. Rev.*, 117(2017), No. 15, p. 10403.
- [5] D.C. Lin, Y.Y. Liu, and Y. Cui, Reviving the lithium metal anode for high-energy batteries, *Nat. Nanotechnol.*, 12(2017), No. 3, p. 194.
- [6] P.B. Zhai, Y. Wei, J. Xiao, *et al.*, *In situ* generation of artificial solid-electrolyte interphases on 3D conducting scaffolds for high-performance lithium-metal anodes, *Adv. Energy Mater.*, 10(2020), No. 8, art. No. 1903339.
- [7] R.J. Braun, B.T. Murray, and J. Soto, Adaptive finite-difference computations of dendritic growth using a phase-field model, *Model. Simul. Mater. Sci. Eng.*, 5(1997), No. 4, p. 365.
- [8] T. Suzuki, M. Ode, S.G. Kim, and W.T. Kim, Phase-field model of dendritic growth, *J. Cryst. Growth*, 237-239(2002), p. 125.

- [9] V. Yurkiv, T. Foroosan, A. Ramasubramanian, R. Shahbazian-Yassar, and F. Mashayek, Phase-field modeling of solid electrolyte interface (SEI) influence on Li dendritic behavior, *Electrochim. Acta*, 265(2018), p. 609.
- [10] Y. Okajima, Y. Shibuta, and T. Suzuki, A phase-field model for electrode reactions with Butler–Volmer kinetics, *Comput. Mater. Sci.*, 50(2010), No. 1, p. 118.
- [11] K.L. Wang, P.C. Pei, Z. Ma, et al., Dendrite growth in the recharging process of zinc–air batteries, *J. Mater. Chem. A*, 3(2015), No. 45, p. 22648.
- [12] Y.H. Zhang, J.F. Qian, W. Xu, et al., Dendrite-free lithium deposition with self-aligned nanorod structure, *Nano Lett.*, 14(2014), No. 12, p. 6889.
- [13] F. Ding, W. Xu, G.L. Graff, et al., Dendrite-free lithium deposition via self-healing electrostatic shield mechanism, *J. Am. Chem. Soc.*, 135(2013), No. 11, p. 4450.
- [14] S.F. Fu, C.Z. Zhu, D. Du, and Y.H. Lin, Enhanced electrocatalytic activities of PtCuCoNi three-dimensional nanoporous quaternary alloys for oxygen reduction and methanol oxidation reactions, *ACS Appl. Mater. Interfaces*, 8(2016), No. 9, p. 6110.
- [15] D. Aurbach, E. Zinigrad, Y. Cohen, and H. Teller, A short review of failure mechanisms of lithium metal and lithiated graphite anodes in liquid electrolyte solutions, *Solid State Ionics*, 148(2002), No. 3–4, p. 405.
- [16] J. Jeon, S. Yoon, T. Park, et al., Tuning glycolide as an SEI-forming additive for thermally robust Li-ion batteries, *J. Mater. Chem.*, 22(2012), No. 39, p. 21003.
- [17] X.B. Cheng, H.J. Peng, J.Q. Huang, R. Zhang, C.Z. Zhao, and Q. Zhang, Dual-phase lithium metal anode containing a polysulfide-induced solid electrolyte interphase and nanostructured graphene framework for lithium–sulfur batteries, *ACS Nano*, 9(2015), No. 6, p. 6373.
- [18] R.L. Sacci, N.J. Dudney, K.L. More, et al., Direct visualization of initial SEI morphology and growth kinetics during lithium deposition by *in situ* electrochemical transmission electron microscopy, *Chem. Commun.*, 50(2014), No. 17, p. 2104.
- [19] S. Choudhury, S. Stalin, D. Vu, et al., Solid-state polymer electrolytes for high-performance lithium metal batteries, *Nat. Commun.*, 10(2019), art. No. 4398.
- [20] W.Y. Li, H.B. Yao, K. Yan, et al., The synergistic effect of lithium polysulfide and lithium nitrate to prevent lithium dendrite growth, *Nat. Commun.*, 6(2015), art. No. 7436.
- [21] L.M. Suo, Y.S. Hu, H. Li, M. Armand, and L.Q. Chen, A new class of solvent-in-salt electrolyte for high-energy rechargeable metallic lithium batteries, *Nat. Commun.*, 4(2013), art. No. 1481.
- [22] Q.D. Wang, Z.P. Yao, C.L. Zhao, et al., Interface chemistry of an amide electrolyte for highly reversible lithium metal batteries, *Nat. Commun.*, 11(2020), art. No. 4188.
- [23] D.C. Lin, Y.Y. Liu, Z. Liang, et al., Layered reduced graphene oxide with nanoscale interlayer gaps as a stable host for lithium metal anodes, *Nat. Nanotechnol.*, 11(2016), No. 7, p. 626.
- [24] G.Y. Zheng, S.W. Lee, Z. Liang, et al., Interconnected hollow carbon nanospheres for stable lithium metal anodes, *Nat. Nanotechnol.*, 9(2014), No. 8, p. 618.
- [25] H. Kwon, J.H. Lee, Y. Roh, et al., An electron-deficient carbon current collector for anode-free Li-metal batteries, *Nat. Commun.*, 12(2021), art. No. 5537.
- [26] J. Pu, J.C. Li, K. Zhang, et al., Conductivity and lithiophilicity gradients guide lithium deposition to mitigate short circuits, *Nat. Commun.*, 10(2019), art. No. 1896.
- [27] R. Pathak, K. Chen, A. Gurung, et al., Fluorinated hybrid solid-electrolyte-interphase for dendrite-free lithium deposition, *Nat. Commun.*, 11(2020), art. No. 93.
- [28] M.S. Kim, J.H. Ryu, Deepika, et al., Langmuir–Blodgett artificial solid-electrolyte interphases for practical lithium metal batteries, *Nat. Energy*, 3(2018), No. 10, p. 889.
- [29] X. Liang, Q. Pang, I.R. Kochetkov, et al., A facile surface chemistry route to a stabilized lithium metal anode, *Nat. Energy*, 2(2017), art. No. 17119.
- [30] Z.Y. Tu, S. Choudhury, M.J. Zachman, et al., Fast ion transport at solid–solid interfaces in hybrid battery anodes, *Nat. Energy*, 3(2018), No. 4, p. 310.
- [31] X.Q. Zhang, X.B. Cheng, X. Chen, C. Yan, and Q. Zhang, Fluoroethylene carbonate additives to render uniform Li deposits in lithium metal batteries, *Adv. Funct. Mater.*, 27(2017), No. 10, art. No. 1605989.
- [32] E. Markevich, G. Salitra, and D. Aurbach, Fluoroethylene carbonate as an important component for the formation of an effective solid electrolyte interphase on anodes and cathodes for advanced Li-ion batteries, *ACS Energy Lett.*, 2(2017), No. 6, p. 1337.
- [33] W.J. Xue, Z. Shi, M.J. Huang, et al., FSI-inspired solvent and “full fluorosulfonyl” electrolyte for 4 V class lithium–metal batteries, *Energy Environ. Sci.*, 13(2020), No. 1, p. 212.
- [34] G.X. Li, Q.Q. Huang, X. He, et al., Self-formed hybrid interphase layer on lithium metal for high-performance lithium–sulfur batteries, *ACS Nano*, 12(2018), No. 2, p. 1500.
- [35] X. Li, J.M. Zheng, X.D. Ren, et al., Dendrite-free and performance-enhanced lithium metal batteries through optimizing solvent compositions and adding combinational additives, *Adv. Energy Mater.*, 8(2018), No. 15, art. No. 1703022.
- [36] S.C. Gu, S.W. Zhang, J.W. Han, et al., Nitrate additives coordinated with crown ether stabilize lithium metal anodes in carbonate electrolyte, *Adv. Funct. Mater.*, 31(2021), No. 28, art. No. 2102128.
- [37] N. Piao, S.F. Liu, B. Zhang, et al., Lithium metal batteries enabled by synergistic additives in commercial carbonate electrolytes, *ACS Energy Lett.*, 6(2021), No. 5, p. 1839.
- [38] C.P. Yang, Y.X. Yin, S.F. Zhang, N.W. Li, and Y.G. Guo, Accommodating lithium into 3D current collectors with a sub-micron skeleton towards long-life lithium metal anodes, *Nat. Commun.*, 6(2015), art. No. 8058.
- [39] Q.B. Yun, Y.B. He, W. Lv, et al., Chemical dealloying derived 3D porous current collector for Li metal anodes, *Adv. Mater.*, 28(2016), No. 32, p. 6932.
- [40] Y. Zhang, Y. Shi, X.C. Hu, et al., A 3D lithium/carbon fiber anode with sustained electrolyte contact for solid-state batteries, *Adv. Energy Mater.*, 10(2020), No. 3, art. No. 1903325.
- [41] J.T. Mao, K.S. Wu, C.K. Ni, et al., Enablement of long-lifespan lithium metal battery via building 3D Li_xGe_y alloy framework, *Electrochim. Acta*, 382(2021), art. No. 138301.
- [42] X.Y. Yue, Q.Y. Zhou, J. Bao, et al., *In situ* construction of lithium silicide host with unhindered lithium spread for dendrite-free lithium metal anode, *Adv. Funct. Mater.*, 31(2021), No. 9, art. No. 2008786.
- [43] M.T. Wan, S.J. Kang, L. Wang, et al., Mechanical rolling formation of interpenetrated lithium metal/lithium tin alloy foil for ultrahigh-rate battery anode, *Nat. Commun.*, 11(2020), art. No. 829.
- [44] Y.Y. Liu, D.C. Lin, P.Y. Yuen, et al., An artificial solid electrolyte interphase with high Li-ion conductivity, mechanical strength, and flexibility for stable lithium metal anodes, *Adv. Mater.*, 29(2017), No. 10, art. No. 1605531.
- [45] R. Xu, X.Q. Zhang, X.B. Cheng, et al., Artificial soft-rigid protective layer for dendrite-free lithium metal anode, *Adv. Funct. Mater.*, 28(2018), No. 8, art. No. 1705838.
- [46] L.P. Wang, L. Zhang, Q.J. Wang, et al., Long lifespan lithium metal anodes enabled by Al₂O₃ sputter coating, *Energy Storage Mater.*, 10(2018), p. 16.
- [47] X.W. Shen, Y.T. Li, T. Qian, et al., Lithium anode stable in air for low-cost fabrication of a dendrite-free lithium battery, *Nat. Commun.*, 10(2019), art. No. 900.
- [48] S.M. Zhang, G.J. Yang, S. Liu, et al., Understanding the drop-

- ping of lithium plating potential in carbonate electrolyte, *Nano Energy*, 70(2020), art. No. 104486.
- [49] Y.Y. Liu, D.C. Lin, Y.Z. Li, *et al.*, Solubility-mediated sustained release enabling nitrate additive in carbonate electrolytes for stable lithium metal anode, *Nat. Commun.*, 9(2018), art. No. 3656.
- [50] J.L. Fu, X. Ji, J. Chen, *et al.*, Lithium nitrate regulated sulfone electrolytes for lithium metal batteries, *Angew. Chem. Int. Ed. Engl.*, 59(2020), No. 49, p. 22194.
- [51] S.M. Zhang, G.J. Yang, Z.P. Liu, *et al.*, Competitive solvation enhanced stability of lithium metal anode in dual-salt electrolyte, *Nano Lett.*, 21(2021), No. 7, p. 3310.
- [52] J.H. Um, K. Kim, J. Park, Y.E. Sung, and S.H. Yu, Revisiting the strategies for stabilizing lithium metal anodes, *J. Mater. Chem. A*, 8(2020), No. 28, p. 13874.
- [53] G.J. Yang, Y.J. Li, S. Liu, S.M. Zhang, Z.X. Wang, and L.Q. Chen, LiFSI to improve lithium deposition in carbonate electrolyte, *Energy Storage Mater.*, 23(2019), p. 350.
- [54] K.Q. Qin, K. Holguin, M. Mohammadiroudbari, *et al.*, Strategies in structure and electrolyte design for high-performance lithium metal batteries, *Adv. Funct. Mater.*, 31(2021), No. 15, art. No. 2009694.
- [55] G.J. Yang, S.M. Zhang, S.T. Weng, *et al.*, Anionic effect on enhancing the stability of a solid electrolyte interphase film for lithium deposition on graphite, *Nano Lett.*, 21(2021), No. 12, p. 5316.
- [56] G.J. Yang, S.M. Zhang, Y.X. Tong, X.Y. Li, Z.X. Wang, and L.Q. Chen, Minimizing carbon particle size to improve lithium deposition on natural graphite, *Carbon*, 155(2019), p. 9.
- [57] C.B. Jin, T.F. Liu, O.W. Sheng, *et al.*, Rejuvenating dead lithium supply in lithium metal anodes by iodine redox, *Nat. Energy*, 6(2021), No. 4, p. 378.
- [58] C.C. Fang, J.X. Li, M.H. Zhang, *et al.*, Quantifying inactive lithium in lithium metal batteries, *Nature*, 572(2019), No. 7770, p. 511.
- [59] Y.J. Li, J.Y. Jiao, J.P. Bi, X.F. Wang, Z.X. Wang, and L.Q. Chen, Controlled deposition of Li metal, *Nano Energy*, 32(2017), p. 241.
- [60] G.J. Yang, Y.J. Li, Y.X. Tong, *et al.*, Lithium plating and stripping on carbon nanotube sponge, *Nano Lett.*, 19(2019), No. 1, p. 494.
- [61] C.P. Yang, Y.G. Yao, S.M. He, H. Xie, E. Hitz, and L.B. Hu, Ultrafine silver nanoparticles for seeded lithium deposition toward stable lithium metal anode, *Adv. Mater.*, 29(2017), No. 38, art. No. 1702714.
- [62] X.Y. Li, G.J. Yang, S.M. Zhang, Z.X. Wang, and L.Q. Chen, Improved lithium deposition on silver plated carbon fiber paper, *Nano Energy*, 66(2019), art. No. 104144.
- [63] H.F. Zheng, Q.F. Zhang, Q.L. Chen, *et al.*, 3D lithiophilic–lithiophobic–lithiophilic dual-gradient porous skeleton for highly stable lithium metal anode, *J. Mater. Chem. A*, 8(2020), No. 1, p. 313.
- [64] Y. Jiang, Z.X. Wang, C.X. Xu, *et al.*, Atomic layer deposition for improved lithiophilicity and solid electrolyte interface stability during lithium plating, *Energy Storage Mater.*, 28(2020), p. 17.
- [65] M.S. Kim, Deepika, S.H. Lee, *et al.*, Enabling reversible redox reactions in electrochemical cells using protected LiAl intermetallics as lithium metal anodes, *Sci. Adv.*, 5(2019), No. 10, art. No. eaax5587.
- [66] H. Ye, Z.J. Zheng, H.R. Yao, *et al.*, Guiding uniform Li plating/stripping through lithium–aluminum alloying medium for long-life Li metal batteries, *Angew. Chem. Int. Ed.*, 58(2019), No. 4, p. 1094.
- [67] P.Y. Gao, H.P. Wu, X.H. Zhang, *et al.*, Optimization of magnesium-doped lithium metal anode for high performance lithium metal batteries through modeling and experiment, *Angew. Chem. Int. Ed.*, 60(2021), No. 30, p. 16506.
- [68] Q.S. Xu, J.J. Lin, C.C. Ye, *et al.*, Air-stable and dendrite-free lithium metal anodes enabled by a hybrid interphase of C₆₀ and Mg, *Adv. Energy Mater.*, 10(2020), No. 6, art. No. 1903292.
- [69] S.M. Zhang, G.J. Yang, Z.P. Liu, *et al.*, Phase diagram determined lithium plating/stripping behaviors on lithiophilic substrates, *ACS Energy Lett.*, 6(2021), No. 11, p. 4118.
- [70] G.J. Yang, X.Y. Li, Z. Guan, *et al.*, Insights into lithium and sodium storage in porous carbon, *Nano Lett.*, 20(2020), No. 5, p. 3836.
- [71] B. Xu, L. Shi, X.W. Guo, *et al.*, Nano-CaCO₃ templated mesoporous carbon as anode material for Li-ion batteries, *Electrochim. Acta*, 56(2011), No. 18, p. 6464.
- [72] V. Velez, G. Ramos-Sánchez, B. Lopez, L. Lartundo-Rojas, I. González, and L. Sierra, Synthesis of novel hard mesoporous carbons and their applications as anodes for Li and Na ion batteries, *Carbon*, 147(2019), p. 214.
- [73] Y. Mao, H. Duan, B. Xu, *et al.*, Lithium storage in nitrogen-rich mesoporous carbon materials, *Energy Environ. Sci.*, 5(2012), No. 7, p. 7950.
- [74] G.J. Yang, Z.P. Liu, S.T. Weng, *et al.*, Iron carbide allured lithium metal storage in carbon nanotube cavities, *Energy Storage Mater.*, 36(2021), p. 459.
- [75] L.F. Wang, M.M. Geng, X.N. Ding, *et al.*, Research progress of the electrochemical impedance technique applied to the high-capacity lithium-ion battery, *Int. J. Miner. Metall. Mater.*, 28(2021), No. 4, p. 538.
- [76] L.Y. Wang, L.F. Wang, R. Wang, *et al.*, Solid electrolyte–electrode interface based on buffer therapy in solid-state lithium batteries, *Int. J. Miner. Metall. Mater.*, 28(2021), No. 10, p. 1584.